NASA/TM—2017-219549

Effect of Angle of Attack on Slope Climbing Performance

Colin M. Creager, Lucas Jones, and Lauren M. Smith
Glenn Research Center, Cleveland, Ohio

December 2017

NASA STI Program . . . in Profile

Since its founding, NASA has been dedicated to the advancement of aeronautics and space science. The NASA Scientific and Technical Information (STI) Program plays a key part in helping NASA maintain this important role.

The NASA STI Program operates under the auspices of the Agency Chief Information Officer. It collects, organizes, provides for archiving, and disseminates NASA's STI. The NASA STI Program provides access to the NASA Technical Report Server—Registered (NTRS Reg) and NASA Technical Report Server—Public (NTRS) thus providing one of the largest collections of aeronautical and space science STI in the world. Results are published in both non-NASA channels and by NASA in the NASA STI Report Series, which includes the following report types:

- TECHNICAL PUBLICATION. Reports of completed research or a major significant phase of research that present the results of NASA programs and include extensive data or theoretical analysis. Includes compilations of significant scientific and technical data and information deemed to be of continuing reference value. NASA counter-part of peer-reviewed formal professional papers, but has less stringent limitations on manuscript length and extent of graphic presentations.

- TECHNICAL MEMORANDUM. Scientific and technical findings that are preliminary or of specialized interest, e.g., "quick-release" reports, working papers, and bibliographies that contain minimal annotation. Does not contain extensive analysis.

- CONTRACTOR REPORT. Scientific and technical findings by NASA-sponsored contractors and grantees.

- CONFERENCE PUBLICATION. Collected papers from scientific and technical conferences, symposia, seminars, or other meetings sponsored or co-sponsored by NASA.

- SPECIAL PUBLICATION. Scientific, technical, or historical information from NASA programs, projects, and missions, often concerned with subjects having substantial public interest.

- TECHNICAL TRANSLATION. English-language translations of foreign scientific and technical material pertinent to NASA's mission.

For more information about the NASA STI program, see the following:

- Access the NASA STI program home page at http://www.sti.nasa.gov

- E-mail your question to help@sti.nasa.gov

- Fax your question to the NASA STI Information Desk at 757-864-6500

- Telephone the NASA STI Information Desk at 757-864-9658

- Write to:
  NASA STI Program
  Mail Stop 148
  NASA Langley Research Center
  Hampton, VA 23681-2199

NASA/TM—2017-219549

Effect of Angle of Attack on Slope Climbing Performance

Colin M. Creager, Lucas Jones, and Lauren M. Smith
Glenn Research Center, Cleveland, Ohio

Prepared for the
Earth and Space Conference
sponsored by the American Society of Civil Engineers
Orlando, Florida, April 11–15, 2016

National Aeronautics and
Space Administration

Glenn Research Center
Cleveland, Ohio 44135

December 2017

This report contains preliminary findings, subject to revision as analysis proceeds.

Level of Review: This material has been technically reviewed by technical management.

Available from

NASA STI Program
Mail Stop 148
NASA Langley Research Center
Hampton, VA 23681-2199

National Technical Information Service
5285 Port Royal Road
Springfield, VA 22161
703-605-6000

This report is available in electronic form at http://www.sti.nasa.gov/ and http://ntrs.nasa.gov/

Effect of Angle of Attack on Slope Climbing Performance

Colin M. Creager, Lucas Jones,* and Lauren M. Smith†
National Aeronautics and Space Administration
Glenn Research Center
Cleveland, Ohio 44135

Abstract

Ascending steep slopes is often a very difficult challenge for off-road vehicles, whether on Earth or on extraterrestrial bodies. This challenge is even greater if the surface consists of loose granular soil that does not provide much shear strength. This study investigated how the path at which a vehicle traverses a slope, specifically the angle that it is commanded to drive relative to the base of the hill (the angle of attack), can affect its performance. A vehicle was driven in loose sand at slope angles up to 15 degrees and angles of attack ranging from 10 to 90 degrees. A novel photogrammetry technique was implemented to both track vehicle motion and create a three-dimensional profile of the terrain. This allowed for true wheel sinkage measurements. The study showed that though low angles of attack result in lower wheel slip and sinkage, the efficiency of the vehicle's uphill motion increased at higher angles of attack. For slopes up to 15 degrees, a 90 degree angle of attack provided the greatest likelihood of successful ascent.

Introduction

One of the greatest challenges for off-road vehicles, whether on Earth or on extraterrestrial bodies, is ascending steep slopes. This is especially difficult when the surface consists of loose granular material, such as sand. This challenge exists currently on Mars when traversing wind-blown sand ripples, and will be an issue for possible future missions to the craters at the Moon's poles. For situations such as these, one option to improve the ability of a vehicle to ascend steep slopes is by implementing vehicle articulation into the method of travel. A number of robotic vehicles have been developed with the ability to control vehicle roll angle when driving cross-slope, thus keeping the chassis level with respect to gravity. Two such examples are the Scarab Rover (Wettergreen, et al., 2010) and the ATHLETE Rover (NASA Jet Propulsion Laboratory, n.d.). These two vehicles use active suspension to raise the wheels on one side of the vehicle while lowering the wheels on the other, allowing the chassis to lean into the slope (Figure 1). Because the weight is distributed more evenly among the wheels, the vehicles have significantly increased traction and stability on steep slopes.

Though this technique has been used to increase the slope-climbing capability of these rovers, the majority of off-road vehicles do not have this option. Other factors, such as the selection of tires, the weight distribution, and the path of ascent, can be varied to improve performance. The purpose of this study was to help determine the most appropriate path of ascent. Specifically, the focus was on the effect of the angle of attack. Angle of attack (β) defines the intended heading of the vehicle relative to the base of the hill. In Figure 2, the angle of attack is the angle relative to the y-axis in the plane of the slope.

The slope angle (θ) is indicated by the arrow in the x-z plane. An angle of attack of 90 degrees would describe a path in a direct uphill direction, while an angle of attack of 0 degrees would indicate a path across the slope with no ascent. It has been generally observed in the field that less wheel slip and sinkage occur at lower angles of attack, but this effect had not previously been quantified. This study serves to quantify the slip and sinkage, but also to evaluate how efficiently the rover ascends a given slope angle as a function of angle of attack, regardless of the final position.

---

*NASA Intern with Lewis Educational and Research Collaborative Internship Project. Currently with General Electric Aviation.

†NASA Intern with Lewis Educational and Research Collaborative Internship Project. Currently with Northrop Grumman Aerospace Systems.

Figure 1.—The (a) Scarab Rover (Wettergreen, et al., 2010) and the (b) ATHLETE Rover (NASA Jet Propulsion Laboratory, n.d.) using active suspension to control vehicle roll when driving cross-slope.

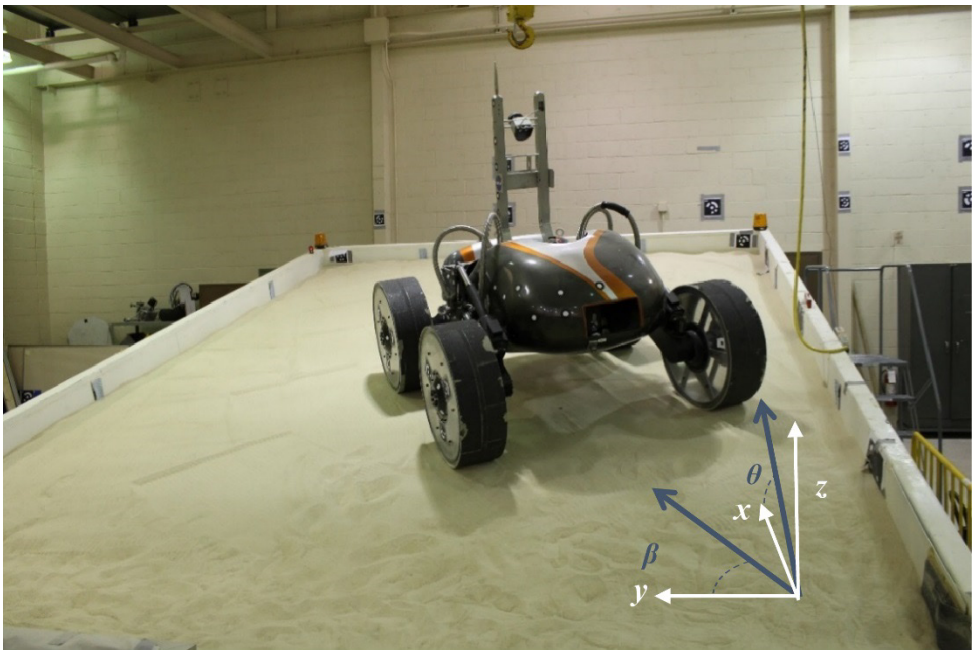

Figure 2.—Scarab driving cross-slope. In this case, the slope angle (θ), is 13 degrees and the angle of attack (β) is 60 degrees.

Test Setup

To evaluate a vehicle's performance on a variety of slope angles, an adjustable tilt-bed at the NASA Glenn Research Center (GRC) was used. The tilt-bed, part of the Simulated Lunar Operations (SLOPE) Laboratory, is approximately 6 m long by 4.5 m wide and filled to a depth of 23 cm with GRC-1 soil. GRC-1 is a unique sand mixture developed to simulate the strength properties of the lunar terrain in Earth ambient conditions (Oravec, Asnani, & Zeng, 2010). To create a challenging and repeatable case, it was prepared to a loose condition before each test by breaking up the soil with shovels and then leveling it to a relatively uniform height with rakes. Cone penetrometer readings were taken in the tilt-bed before each test; by combining the cone penetrometer data with the laboratory characterization of GRC-1 (Oravec, Asnani, & Zeng, 2010), mechanical properties of GRC-1 in this loosened state were estimated (Table 1).

TABLE 1.—PROPERTIES OF GRC-1 IN THE LOOSE STATE USED FOR TESTING (ORAVEC, ASNANI, & ZENG, 2010). D_{10} AND D_{60} REPRESENT THE DIAMETER OF WHICH 10 AND 60 PERCENT OF THE SOIL PARTICLES ARE SMALLER, RESPECTIVELY

Particle shape	Sub-angular
D_{10} (mm)	0.094 mm
D_{60} (mm)	0.390 mm
Specific gravity	2.583
Mean cone index gradient	2.5 (±0.5) kPa/mm
Bulk density (g/cc)	1.63 g/cc
Relative density	11%
Friction angle (deg)	31.5 deg
Cohesion (kPa)	~0 kPa

The Scarab Rover

The Scarab Rover (Figure 3) served as the test vehicle for this study, though its active suspension was not incorporated. Instead the height of the chassis and the distance between front and rear axles were held constant. The total mass of the vehicle was 400 kg and the load was fairly even among all four tires when on flat ground. Rigid tires were chosen for this study because of their simplicity as well as relevancy to current planetary roving vehicles. The tires had a diameter of 71 cm and a width of 18 cm.

Photogrammetry methods were employed to track the test vehicle's movements throughout a test. Coded two-dimensional targets were applied to both of the left tires as shown in Figure 3. During each test, a pair of cameras mounted at a fixed distance and angle apart would trigger every 2 s capturing a set of stereo images covering the vehicle's entire path. Based upon the known orientations of the cameras, a software developed by Gom (Gom Optical Measuring Techniques, n.d.) called Pontos would then identify the three-dimensional coordinates of each coded target for each pair of images. This information could then be used to chart the rigid body motion of each wheel, as well as the motion of the vehicle as a whole. The cameras had an image resolution of 4272×2848 pixels, which resulted in a spatial resolution between 1.5 and 2 mm, depending on the focal distance. The calibration process yielded an average deviation between computed and actual coordinates of 0.196 pixels (approximately 0.29 to 0.39 mm).

Terrain Mapping for Sinkage Measurements

Though the soil was leveled by hand with rakes before each test, there were still slight variations in terrain height throughout the tilt-bed. Because of this, the true sinkage of the tires could not be determined by the position of the wheels alone; the relative distance between the wheel center and the terrain had to be found. In order to map the terrain, a novel photogrammetry technique was implemented, similar to the method utilized for tracking the vehicle. After the terrain was verifiably prepared to the loose condition previously described, the tilt-bed was raised to a desired slope angle (θ), as indicated by an inclinometer on the side of the bed. Once in place, a speckled dot pattern was projected on to the terrain that encompassed the area in which the test vehicle would be driven (Figure 4). A pair of images was taken of the tilt-bed and the projected dots using the two cameras. Another software called Aramis, also developed by Gom (Gom Optical Measuring Techniques, n.d.), would then identify unique sections of the pattern and assign them each a discrete set of three-dimensional coordinates. The location of each point was averaged over a 19×19 pixel square, with the centers of the squares spaced 15 pixels apart (22.5 to 30 mm apart). All of the points would then be combined into a "point cloud" (see Figure 5) that served as a digital profile of the terrain's surface.

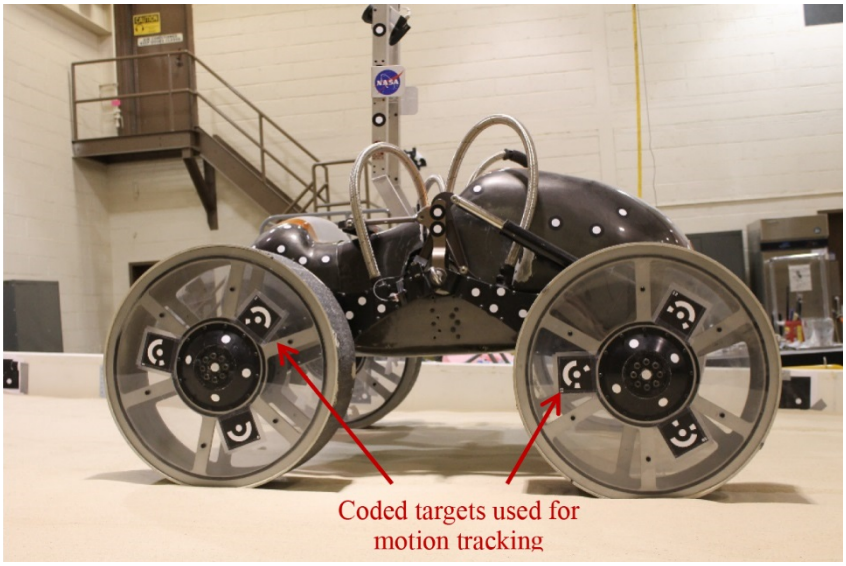

Figure 3.—Scarab with 71 cm rigid wheels.

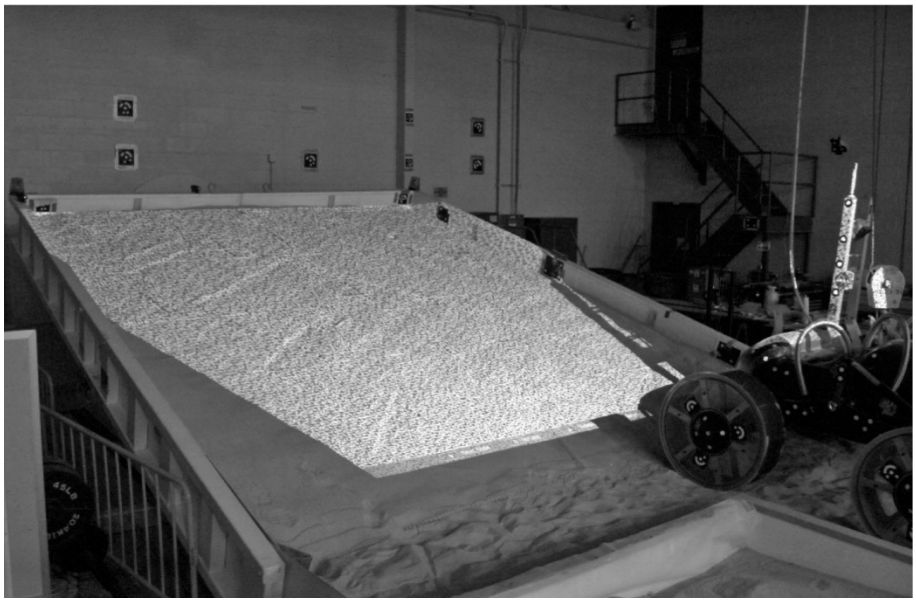

Figure 4.—The dot pattern is projected onto the tilt bed before a test in order to create a three-dimensional profile of the surface using photogrammetry.

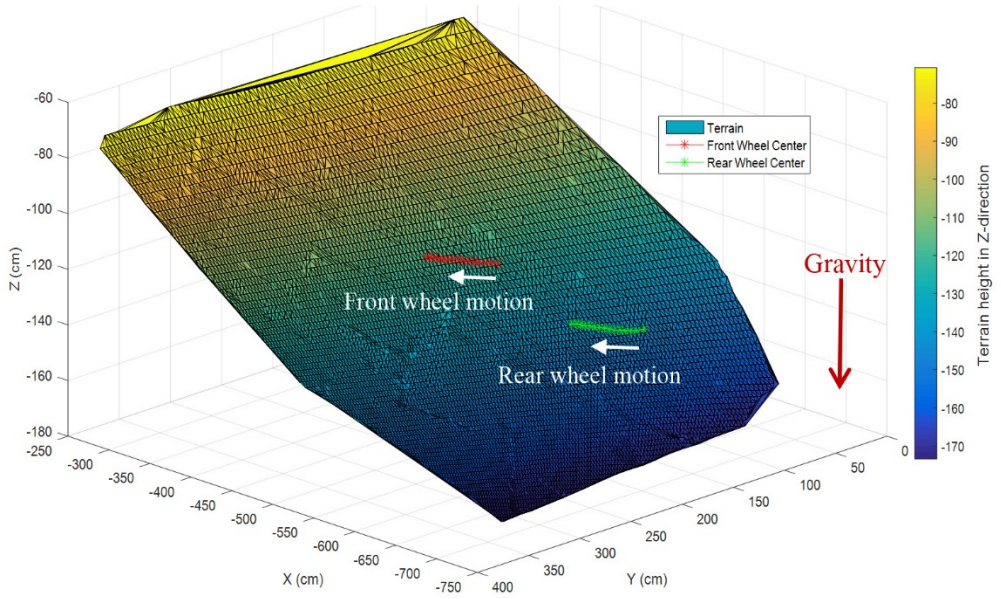

Figure 5.—The position of each wheel center plotted in the same coordinate system as the terrain point cloud. The z-axis has been scaled to highlight small changes in terrain height.

After this initial image pair was taken, the vehicle was lifted and set in place with a crane. Laser range-finders were used to help orient the vehicle to the target angle of attack, though slight settling occurred in the soil during this placement procedure; thus, the actual starting angle of attack typically varied slightly from the target value. For each test, the vehicle was driven with a constant wheel rotational speed of 0.13 rad/s for 30 s (see Figure 6). When driving on a slope angle of 9 degrees with a starting angle of attack of 10 degrees, Scarab could only drive for approximately 30 s before nearing the opposite wall of the tilt bed. In order to allow for an accurate comparison between tests, this drive time was used for each condition. During the test, images were captured from the two cameras every 2 s and both voltage and current were recorded from sensors on the test vehicle's power bus.

To ensure the point cloud data and the wheel position data were in the same coordinate system, coded targets were mounted on the walls of the laboratory, and were used as common reference positions (see Figure 6). It was also assumed that these targets were mounted on a plane containing the gravity vector, with the bottom two targets representing a line perpendicular to gravity. The point cloud of the surface and the wheel position data at each time step were then plotted together as seen in Figure 5. The z-axis represents the vertical (in the direction of gravity), the x-axis represents the direction towards the far end of the tilt-bed, and the y-axis represents the direction across the tilt-bed.

A best-fit plane was then created from the surface point cloud data. The angle of this plane about the y-axis was taken to be the slope angle (θ) of the terrain. This value was typically within 1 degree of the target angle set by the inclinometer on the side of the bin. A rotation matrix was created based upon this angle and applied to both the point cloud and wheel position data so that the vehicle's motions could be normalized to the terrain. The normalized results are shown in Figure 7. It should be noted that the scale of the z-axis is much smaller than the other axes to highlight small changes in terrain height.

In this new normalized coordinate system, the z-axis now represents the direction normal to the tilt-bed, and the x-axis represents the direction uphill. At each time step, a search algorithm was implemented to find the closest point in the point cloud to each wheel center position. The z-coordinate of this point, as well as the five points before and after this one along the y-axis (approximately a 10 to 15 cm length of terrain), were averaged to get a local terrain height value. The distance along the z-axis between the

wheel center and this terrain height value was calculated and represented as $\Delta Z_{\text{front/rear}}$. Because the tires were rigid, absolute sinkage was then computed as

$$z_{\text{front/rear}} = \Delta Z_{\text{front/rear}} - r \tag{1}$$

where z = sinkage and r = tire radius. According to this convention, when the tires were below the terrain surface the sinkage was a negative number.

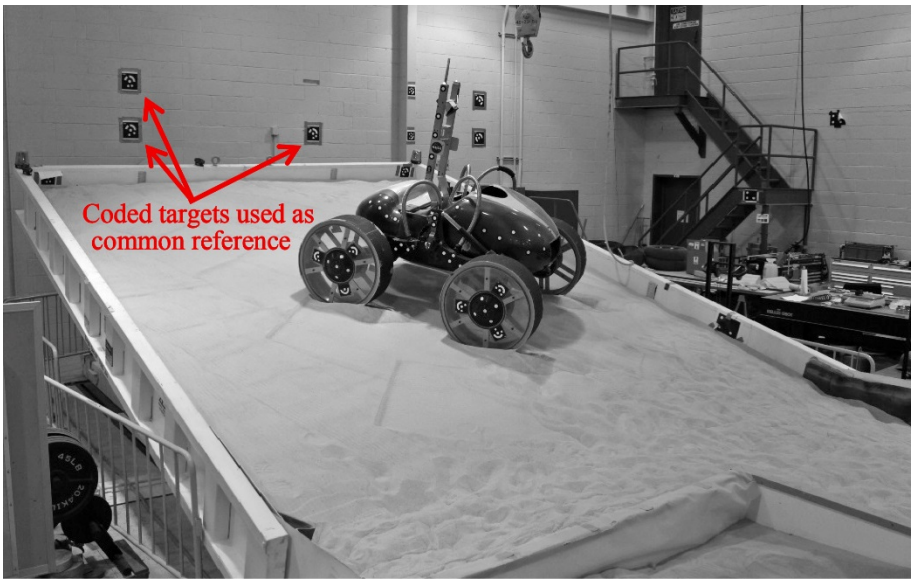

Figure 6.—Cameras tracked the targets on Scarab's wheels to compute vehicle motion. The targets on the walls were used as a common reference between the sets of images.

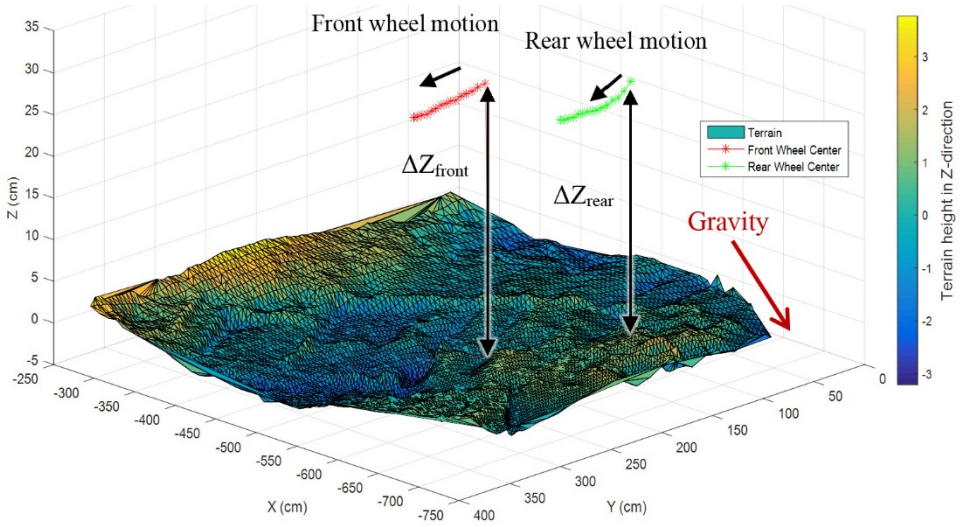

Figure 7.—The coordinates for the wheel centers and terrain surface normalized to a best-fit plane through the surface point cloud. The z-axis has been scaled to highlight small changes in terrain height.

Metrics Used for Evaluation

In addition to the vehicle's trajectory and change in orientation, other metrics were used to evaluate vehicle performance as a function of angle of attack. Wheel sinkage, as defined above, provides insight into the likelihood of a vehicle becoming entrenched in the terrain. For a majority of these tests, sinkage continued to increase, never reaching a steady depth. Because of this, the changes in sinkage throughout each tested were evaluated. The maximum sinkage per test (or over 30 s of travel) was also used for comparison.

Wheel slip (i) is related to sinkage, though was fairly constant throughout each test. Slip is used to quantify the shear displacement beneath a wheel and is typically defined by the following equation (Meyer, et al., 1977):

$$i = \left(\frac{r_{\text{eff}} w - v}{r_{\text{eff}} w} \right) \times 100\% \tag{2}$$

where v is the velocity of the vehicle in a given direction, r_{eff} is the effective radius of the tire, and w is the rotational speed of the wheel in rad/s. If slip is assumed to be constant over a given time period, the equation can be rewritten as follows:

$$i = \left(\frac{r_{\text{eff}} \varphi - d}{r_{\text{eff}} \varphi} \right) \times 100\% \tag{3}$$

where d is the distance traveled in a given direction and φ is the total rotations of the wheel in radians. For a case where $i = 0$, this equation can be rearranged to solve for r_{eff}:

$$r_{\text{eff}} = \frac{d}{\varphi} \tag{4}$$

To determine the effective radius of the rigid tires used in this study, the test vehicle was driven on a non-slip surface ($i = 0$) while measuring the distance traveled and total wheel rotation. This resulted in an effective radius of 35.6 cm.

For these tests, wheel slip was calculated at each time step in the direction the vehicle was oriented at that time. For a given time step n, the change in position between n and $n+1$ for each wheel was measured. The component of this distance in the direction that the vehicle was oriented at n was then used to compute slip at n. This distance is represented by d_n in Figure 8.

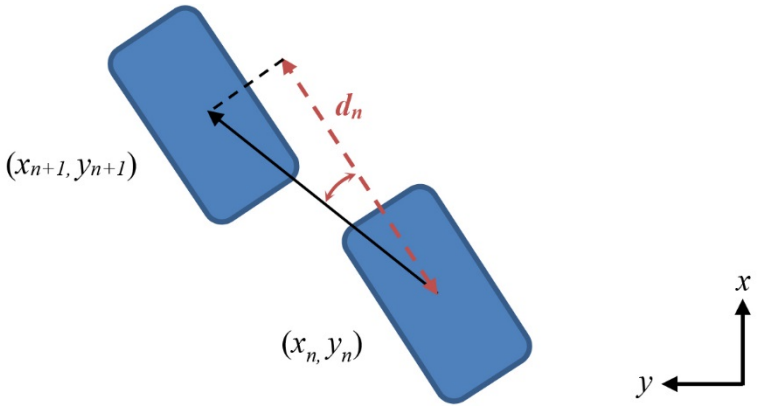

Figure 8.—The front wheel shown at two consecutive time steps (n and $n+1$). d_n represents the distance used to compute wheel slip at n.

Though wheel slip was computed at each time step, the values were fairly constant throughout each test; thus an average slip value was ultimately computed for each run and used for evaluation.

Power number (*PN*) provides information on how efficiently the vehicle travels to the top of a slope, regardless of the distance traveled cross-slope. It is calculated as follows:

$$PN = \frac{E}{Wd_x} \tag{5}$$

where E is the total electrical energy consumed by the vehicle for a given time period, W is the vehicle weight, and d_x is the distance traveled uphill (along the x-axis). It should be noted that this is a modified version of the standard power number metric (Meyer, et al., 1977) which is generally used in drawbar pull testing where the vehicle can only drive in a straight line. Because only the component of travel in the uphill direction is taken into account, this metric can be used to compare the energy required to climb a given slope angle for various angles of attack. The total electrical energy was computed from the voltage and current coming out of the vehicle's power bus. For this study, one value for power number was computed per test.

Results and Discussion

A total of 16 different cases were evaluated, using combinations of four slope angles (θ) and four angles of attack (β). For this study, 15 degrees was chosen as the maximum slope angle because it represented a very challenging case in which the rover was not able to ascend successfully at all angles of attack. The actual slope angles were determined by the best-fit plane of the surface point cloud; the actual angles of attack were calculated by the starting orientation of the test vehicle relative to the y-axis in the plane of the terrain for each test. A test was also conducted at a slope angle of 0 degrees for reference. It should be noted that due to the time-intensive nature of both the test preparation and post-processing, repeat tests were not conducted unless there was cause to do so. If a test for a specific condition was repeated (due to a known error in measurement or testing procedures), only the data for the repeat test are shown here.

For each test, the positions of both the left front and left rear wheels were plotted in a three-dimensional space along with the surface point cloud, where the z-axis is parallel to gravity (example shown in Figure 5). Then, as discussed above, a best fit plane of the point cloud data was produced and all of the position data sets (for the terrain profile and wheels) were then normalized to this plane and plotted in a new coordinate system (Figure 7). In this modified coordinate system, the x-axis represents the direction uphill, the y-axis represents the direction cross slope, and the z-axis is normal to the terrain.

The normalized wheel position data for each test can be seen in Figure 9. There are four graphs, one for each target slope angle and each includes all four angles of attack. Each data point represents 2 s of movement beginning in the lower right corner. The position data has been shifted so that each test begins at (0,0) to allow for easier comparison. Colored lines connecting the front and rear wheels at each step were included to indicate vehicle position and orientation. The dashed lines represent the target angles of attack.

The space between each data point is proportional to the total distance traveled over each 2 s interval. Points spaced closely together indicate high wheel slip. The change in angle of the colored lines over time indicate the amount of vehicle yaw (rotation about the z-axis); and the space between the colored lines indicates the amount of side slip. Progress uphill can easily be identified by the path of the wheels along the x-axis.

It can be seen that aside from the cases where β = 90 degrees, the vehicle's actual trajectory always trends away from its intended path in the downward direction. This becomes more prominent at higher slope angles and at lower angles of attack. In fact, when driving at β = 10 degrees, the vehicle actually made no progress uphill for slope angles greater than 9 degrees. On the 15 degree slope, the vehicle did not make any positive progress for β = 10 degrees or 30 degrees. Though vehicle yaw (rotation about the z-axis) did not change much in any of these cases, there was significant side slip at all angles of attack other than 90 degrees.

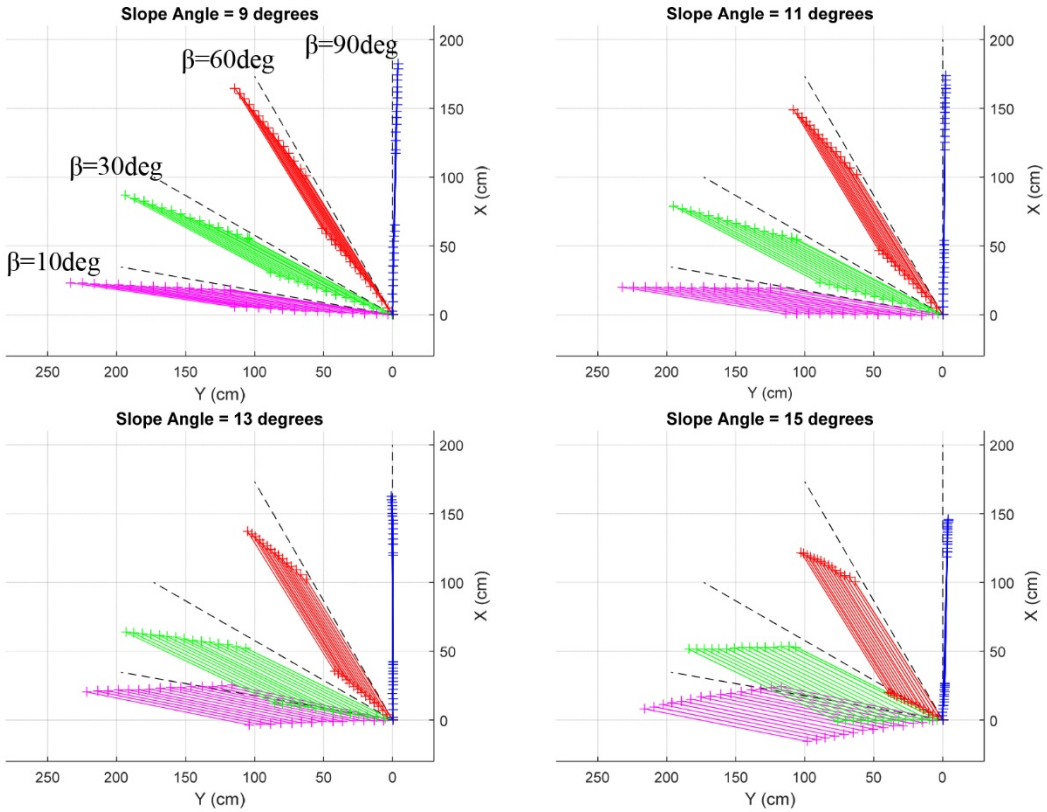

Figure 9.—The positions of the front and rear wheels for each case plotted on the normalized x-y plane.

In Figure 10, the trajectory of the vehicle center (taken as the point directly between the front and rear wheels) has been plotted. The sinkage of the rear wheel at each position was also indicated by the color of the marker, ranging from 0 to –8 cm. Only the rear wheel sinkage has been displayed since it was consistently greater than that of the front wheel and therefore represented the worst case. From this data, there is a clear relationship between angle of attack and sinkage; the wheels sank far less into the ground at the shallower angles of attack than at steeper angles of attack.

As seen in Figure 11, wheel slip definitively increased with both slope angle and angle of attack. Though wheel slip was calculated for both wheels at each time step, the values were very similar (less than 0.5 percent difference between front and rear), thus only the rear wheel slip is shown here. It was predicted that wheel slip would increase with slope angle because greater thrust is needed to climb steeper slopes. Increased thrust generation requires increased soil displacement, thus greater wheel slip.

Wheel slip can be a good indicator of how much a vehicle will continue to sink over time; however, it does not tell the whole story of how efficiently a vehicle can ascend a given slope. Because power number only takes into account the vehicle's motion in the uphill direction, it provides insight into the ability of the vehicle to reach the top of the hill while taking power consumption into account. The power numbers associated with each angle of attack at various slope angles are plotted in Figure 12. A higher power number corresponds with more energy required to ascend a given slope. For slope angles that the test vehicle were not able to ascend, the power number approached infinity. In fact, the 10 degree angle of attack case is not shown here because the vehicle never made uphill progress for slope angles above 9 degrees; thus the power number would have been infinite or negative. For β = 30 degrees, Scarab was unable to make uphill progress at a slope angle of 15 degrees. For the most part, there was a clear relationship between angle of attack and power number; as the angle of attack went up, so did the vehicle's climbing efficiency. The only ambiguity was between the 60 and 90 degree angle of attack tests, where there was no noticeable difference in power number at the lower slope angles (11 degrees and below).

It should be noted that even though no tests were conducted at slope angles greater than 15 degrees, the slope angle versus PN curves appear to diverge as slope angle goes up. This trend would suggest that greater angles of attack would still result in more efficient climbing at higher slope angles, though more testing would be needed to verify this.

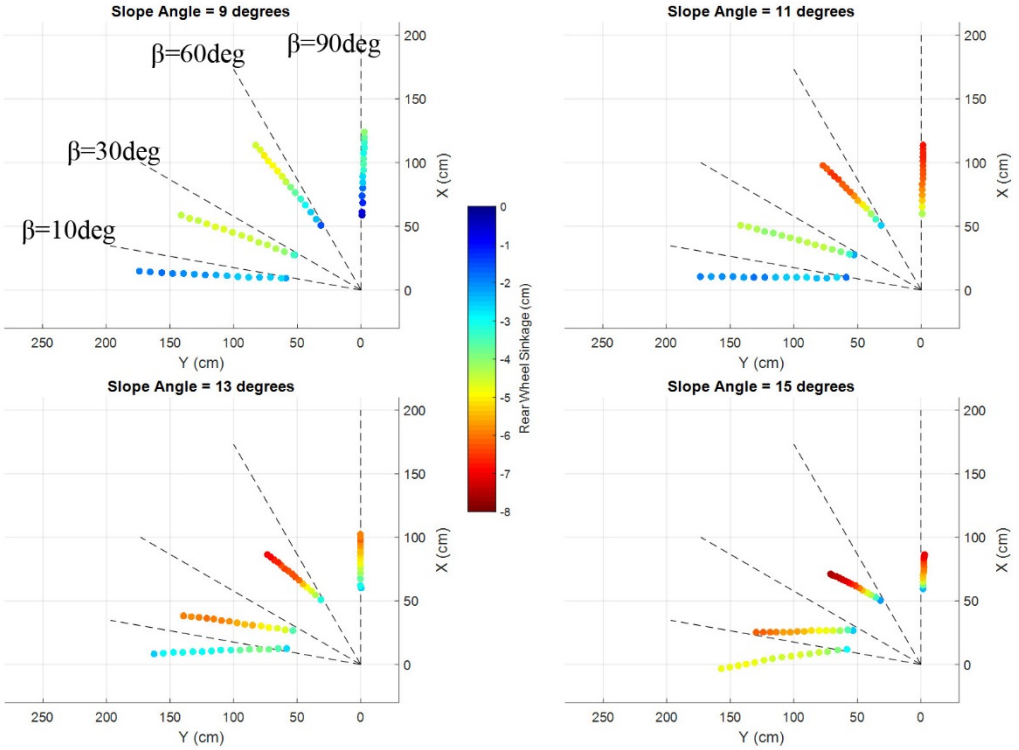

Figure 10.—The position of the vehicle center plotted on the normalized X-Y plane. Color is used to indicate the sinkage (*z*) of the rear wheel.

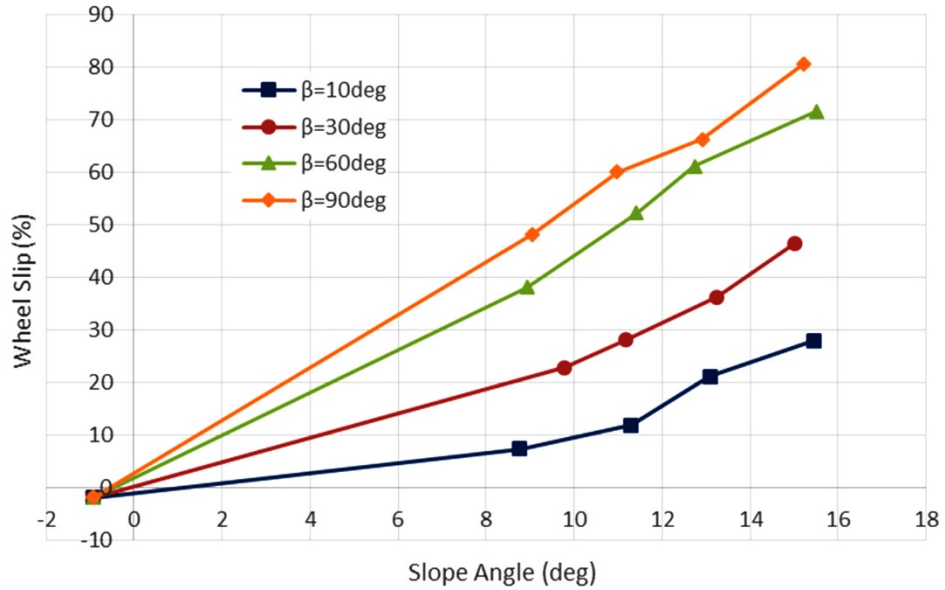

Figure 11.—Wheel slip (*i*) as a function of slope angle.

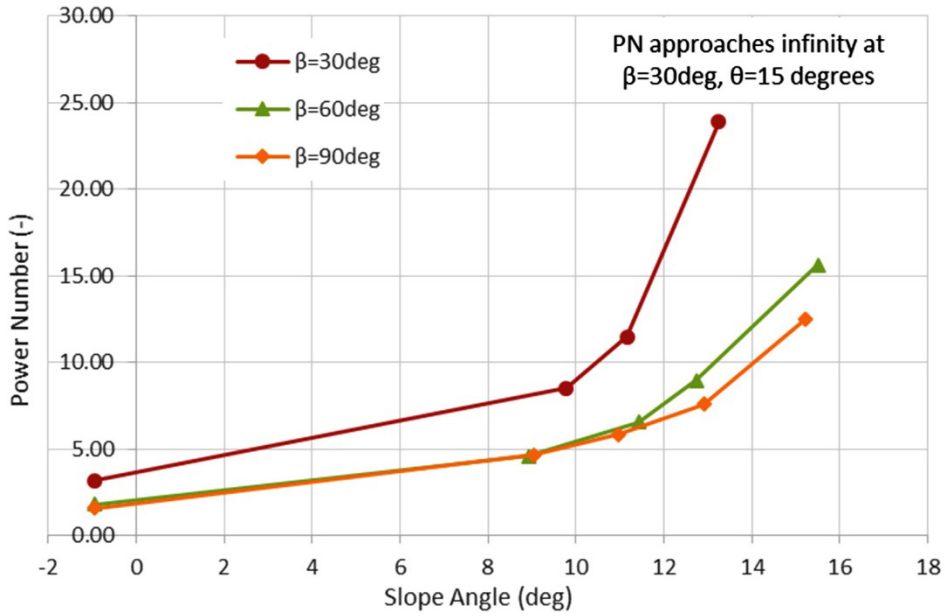

Figure 12.—Power number as a function of slope angle. At 10 degrees angle of attack, the vehicle made zero or negative progress for slope angles greater than 9 degrees, producing an infinite or negative power number.

Conclusions

The following conclusions were made as a result of this study:

1. For the conditions used in this study (a 4×4 vehicle with rigid wheels and fixed suspension driving on loose granular soil), the angle of attack had a very noticeable impact on the vehicle's performance when climbing a hill. Less sinkage occurred when starting at lower angles of attack; however the vehicle's driving efficiency uphill was superior at higher angles of attack.
   a. The vehicle had a higher likelihood of successful traversal of steeper slopes when using higher angles of attack. When starting with an angle of attack of 10 degrees, the vehicle was not able to ascend slopes 11 degrees or higher.
2. A path of traversal directly uphill (β = 90 degrees) produced the most efficient path to reach the top of a hill and also provided the highest likelihood of successful ascent for the slope angles tested. It is recommended for conditions similar to the ones used in this study to use an angle of attack of 90 degrees when driving uphill if the final vehicle position is not important.
3. It is possible that as wheel slip becomes great enough to cause vehicle entrapment, lower angles of attack might result in better performance uphill. This does not appear to be the case based upon the trends of the power number versus slope angle curves. However, there is not enough data from this study to determine a definitive answer and further testing at steeper slopes is recommended.
4. Further study should be conducted to quantify the benefit, under the same terrain conditions, of vehicle articulation, such as controlling the roll angle of the chassis so that it is always level with respect to gravity.

References

Gom Optical Measuring Techniques. (n.d.). *Pontos Software*. Retrieved 2013, from http://www.gom.com/3d-software/pontos-software.html

Meyer, M. P., Ehrlich, I. R., Sloss, D., Murphy, J. N., Wismer, R. D., & Czako, T. (1977). International Society for Terrain-Vehicle Systems Standards. *Journal of Terramechanics*, *14*(3, pgs 153–182), vol. 14, no. 3, pgs. 153–182.

NASA Jet Propulsion Laboratory. (n.d.). *JPL Robotics*. Retrieved from The ATHLETE Rover: http://www-robotics.jpl.nasa.gov/systems/system.cfm?System=11

Oravec, H., Asnani, V., & Zeng, X. (2010). Design and characterization of GRC-1: A soil for lunar terramechanics testing in Earth-ambient conditions. *Journal of Terramechanics, 47*(6), 361–377.

Wettergreen, D., Moreland, S., Skonieczny, K., Jonak, D., Kohanbash, D., & Teza, J. (2010). Design and field experimentation of a prototype Lunar prospector. *International Journal of Robotics Research*, vol. 29 no. 12 pg. 1550–1564.